Available online at www.sciencedirect.com
ScienceDirect
Remote Sensing of Environment 112 (2008) 375–390
Remote Sensing of Environment
www.elsevier.com/locate/rse

Aircraft based soil moisture retrievals under mixed vegetation and topographic conditions

R. Bindlish [a,*], T.J. Jackson [b], A. Gasiewski [c], B. Stankov [d], M. Klein [c], M.H. Cosh [b], I. Mladenova [e], C. Watts [f], E. Vivoni [g], V. Lakshmi [e], J. Bolten [b], T. Keefer [h]

[a] SSAI, USDA ARS Hydrology and Remote Sensing Lab, USA
[b] USDA ARS Hydrology and Remote Sensing Lab, USA
[c] University of Colorado, USA
[d] NOAA Earth Sciences Research Laboratory, USA
[e] University of South Carolina, USA
[f] University of Sonora, Mexico
[g] New Mexico Institute of Mining and Technology, USA
[h] USDA ARS Southwest Watershed Research Center, USA

Received 11 July 2006; received in revised form 19 December 2006; accepted 15 January 2007

Abstract

An unresolved issue in global soil moisture retrieval using passive microwave sensors is the spatial integration of heterogeneous landscape features to the nominal 50 km footprint observed by most low frequency satellite systems. One of the objectives of the Soil Moisture Experiments 2004 (SMEX04) was to address some aspects of this problem, specifically variability introduced by vegetation, topography and convective precipitation. Other goals included supporting the development of soil moisture data sets that would contribute to understanding the role of the land surface in the concurrent North American Monsoon System. SMEX04 was conducted over two regions: Arizona — semi-arid climate with sparse vegetation and moderate topography, and Sonora (Mexico) — moderate vegetation with strong topographic gradients. The Polarimetric Scanning Radiometer (PSR/CX) was flown on a Naval Research Lab P-3B aircraft as part of SMEX04 (10 dates of coverage over Arizona and 11 over Sonora). Radio Frequency Interference (RFI) was observed in both PSR and satellite-based (AMSR-E) observations at 6.92 GHz over Arizona, but no detectable RFI was observed over the Sonora domain. The PSR estimated soil moisture was in agreement with the ground-based estimates of soil moisture over both domains. The estimated error over the Sonora domain (SEE = 0.021 cm^3/cm^3) was higher than over the Arizona domain (SEE = 0.014 cm^3/cm^3). These results show the possibility of estimating soil moisture in areas of moderate and heterogeneous vegetation and high topographic variability.

Keywords: Soil moisture; Microwave; AMSR-E; Hydrology

1. Introduction

Surface boundary conditions play an important role in initiation and maintenance of the North American Monsoon System (NAMS), which controls summer precipitation over much of interior North America (Barlow et al., 1998). The most important surface boundary conditions are sea surface temperature and land surface wetness and temperature. One of the goals of the North American Monsoon Experiment (NAME) is to test the hypothesis that soil moisture conditions in southwestern U.S. and northern Mexico and snow extent in northwestern U.S. control the onset and intensity of the NAMS (Higgins et al., 2006). This information would lead to improved prediction of warm season precipitation. The soil moisture conditions and the snow extent are typically out of phase with each other. The concurrent conditions that typify NAMS are out of phase surface wetness and temperature in the southwestern U.S. and northern Mexico, on

* Corresponding author. USDA ARS Hydrology and Remote Sensing Lab, 104 Bldg. 007, BARC-West, Beltsville, MD 20705, USA. Tel.: +1 301 504 5363.
E-mail address: rajat.bindlish@ars.usda.gov (R. Bindlish).

0034-4257/$ - see front matter © 2007 Elsevier Inc. All rights reserved.
doi:10.1016/j.rse.2007.01.024

one hand, and in the U.S. Great Plains, on the other (Higgins et al., 2006). The influence of the land surface is relayed through surface evaporation and associated surface cooling (dependent on soil moisture), terrain, and vegetation cover. Soil moisture can change dramatically after heavy rain events. Increased soil moisture after precipitation results in increased evapotranspiration between storm events. This increase may contribute to enhanced convection and further precipitation. Soil moisture can vary both spatially, due to topography, soil, vegetation and precipitation variability, and temporally, due to differences in soil physical characteristics that control drainage and accumulated evapotranspiration.

Soil Moisture Experiment 2004 (SMEX04) builds on preceding experiments by focusing specifically on topography, vegetation and strengthening the soil moisture components of the North American Monsoon Experiment (NAME). An accurate characterization of spatial and temporal variability of soil moisture is critical to NAME in three ways;

(1) The spatial and temporal patterns of soil moisture estimated from remote sensing (by aircraft so as to provide high spatial resolutions) can be used for initialization and/or updating of the boundary conditions for the land surface component of land-atmosphere models.
(2) The spatial and temporal patterns of soil moisture can be used for validation of land surface model outputs, and to discern the relationship between soil moisture and warm season precipitation and associated feedback mechanisms.
(3) Aircraft-based soil moisture mapping can provide a basis for model-based extrapolation over large areas, using methods developed under Land Data Assimilation Systems (LDAS) and Advanced Microwave Scanning Radiometer (AMSR-E) validation studies. For the continental scale domains, satellite retrievals using the Aqua AMSR-E are most appropriate, and have been validated using aircraft observations as well as in-situ measurements from networks such as the Little Washita watershed (Jackson et al., 2005).

The Soil Moisture Experiment 2004 (SMEX04) focused on providing these critical soil moisture products using the new generation of satellite sensors supported with aircraft observations. At the same time it contributed to the validation of these products and investigated the effects of key land surface features and the potential of new technologies for soil moisture mapping.

Field experiments in support of remote sensing, hydrology and climate have included catchments throughout North America (Little Washita, Oklahoma: Washita 92, Washita 94, SGP97, SGP99, SMEX03; Little River, Georgia: 2000, SMEX03; Walnut Creek, Iowa: SMEX02). These experiments have been intensive efforts ranging from one to six weeks in duration. The basic approach used in these experiments has been to collect ground-based samples of soil moisture in conjunction with aircraft flights that coincided with satellite overpasses. The aircraft instruments operate in low frequency microwave wavebands that are well suited for the measurement of soil moisture. The aims of these experiment have been to validate remotely sensed data from aircraft and/or space-borne microwave sensors, to map the spatial and temporal variability of soil moisture, establish the relationship of soil moisture to vegetation and the near-surface atmospheric characteristics, and the collection of in-situ gravimetric soil moisture data for validation of soil moisture networks, and to investigate the impact of antecedent soil moisture on land surface hydrological models used to simulate the watershed at pre-specified spatial and temporal resolutions.

Soil moisture retrieval algorithms utilizing AMSR-E data have been proposed but not rigorously evaluated since there are few data sets available for this purpose (Jackson, 1993; Koike et al., 2000; Njoku & Li, 1999; Paloscia et al., 2001; Njoku et al., 2003). This lack of data is a critical issue that needs to be addressed for both algorithm development and validation. As part of ongoing efforts to validate soil moisture products from AMSR-E, several watershed sites in the U.S. have been instrumented to provide continuous long-term observations of surface soil moisture and temperature. The Aqua calibration/validation plan includes intensive experiments to calibrate and validate these sites using ground and aircraft observations. One of the sites is the Walnut Gulch Experimental Watershed near Tombstone Arizona (Cosh et al., 2008-this issue). For SMEX04, ground observations of soil moisture and related variables were collected in conjunction with airborne measurements with the Polarimetric Scanning Radiometer (PSR) with its C-and X-band scanheads (PSR/CX). PSR/CX has the same lowest frequencies as the AMSR-E instrument (6.92 and 10.7 GHz).

This paper focuses on the results from the SMEX04 aircraft campaign involving the PSR and relationships between the aircraft and satellite observations. The NAME region includes a wide range of arid to semi-arid conditions and heterogeneous topography that allow us to develop and evaluate soil moisture retrieval algorithms using microwave remote sensing in regions with moderate to significant topographic variation, which is a unique aspect of this experiment. The presence of both arid and semi-arid conditions in the same region permits robust testing of the algorithm for varying vegetation conditions. One of the objectives of the PSR observations was to validate the brightness temperature and soil moisture products from the Aqua AMSR-E instrument. The PSR measurements will also allow us to check and evaluate techniques for mitigating the effect of Radio Frequency Interference (RFI) on the brightness temperature observations. These studies will contribute to the design of both algorithms and sensors for future space platforms as well as the broader science issues of NAME.

2. SMEX04 description

SMEX04 involved four complementary elements that together contribute to validation of both the aircraft and satellite products: an in-situ soil moisture network, aircraft mapping of soil moisture, intensive in-situ sampling concurrent with aircraft missions, and satellite products. The timing of SMEX04 and the NAME Enhanced Observing Period were driven by the NAMS. Rainfall statistics clearly indicated that the field experiment

Table 1
Dates of SMEX04 PSR missions and AMSR-E coverage over AZ and SO domains

	Aircraft mission		Satellite
Date (August 2004)	AZ	SO	AMSR-E
5	X	X	X
6			
7		X	X
8	X	X	
9	X	X	X
10	X	X	X
11			
12	X	X	X
13	X	X	
14		X	X
15			
16			X
17			
18			X
19			X
20			
21			X
22			
23			X
24	X	X	
25	X	X	X
26	X	X	X

should be between mid-July and mid-August, when the number of rainy days is large and the possibility of having flights prior to and subsequent to heavy rainfall is high. Due to problems involving flight readiness of the aircraft, the start of SMEX04 was delayed until the beginning of August and was interrupted by a subsequent aircraft failure. The flight dates and coverage are summarized in Table 1.

Within the much larger NAME domain, two regional study sites (~50 km by ~75 km) were established: Walnut Gulch, Arizona (AZ) and Sonora, Mexico (SO). The NAMS dominates the precipitation regime with slightly more than 60% of the annual total falling during July, August and September. Summer events are localized short-duration, high-intensity convective thunderstorms driven by the intense solar heating of the land surface and moisture inputs from the Gulf of Mexico and Gulf of California.

The general vegetation conditions for the two sites are clearly illustrated in the Landsat image shown in Fig. 1. The false color composite of the SMEX04 domain indicates low vegetation conditions before the start of the monsoon (July 11, 2004 image). The false color composite for July 29, 2004 shows the growth in vegetation after the onset on the monsoons, indicated by the increase in red areas. The vegetation cover decreased at the end of the monsoon period (August 30, 2004– coinciding with the end of the SMEX04 experiment). This image also shows the difference in vegetation biomass over the two SMEX04 study areas. The AZ domain had lower vegetation biomass than the SO domain. The SO domain also had greater topographic variability than the AZ domain.

2.1. Arizona study region

The Arizona (AZ) study area was 50 by 75 km covering six Ease Grids. The core of the AZ study area is the USDA-ARS Walnut Gulch Experimental Watershed (WGEW) (http://tucson.ars.ag.gov/unit/watersheds/wgew.htm). The WGEW encompasses 150 km^2 and is representative of brush and grass covered rangeland found throughout the semi-arid southwest. Elevation of the watershed ranges from 1250 m to 1585 m MSL. Shrub grazing is the primary land use. The WGEW lies in the transition zone between the Sonoran and the Chihuahuan Deserts. The climate is classified as semi-arid, with mean annual temperature at Tombstone, Arizona of 17.7 °C and mean annual precipitation of 350 mm. Soils on the WGEW are generally well-drained, calcareous, gravelly loams with large percentages of rock and gravel at the soil surface. Soil surface

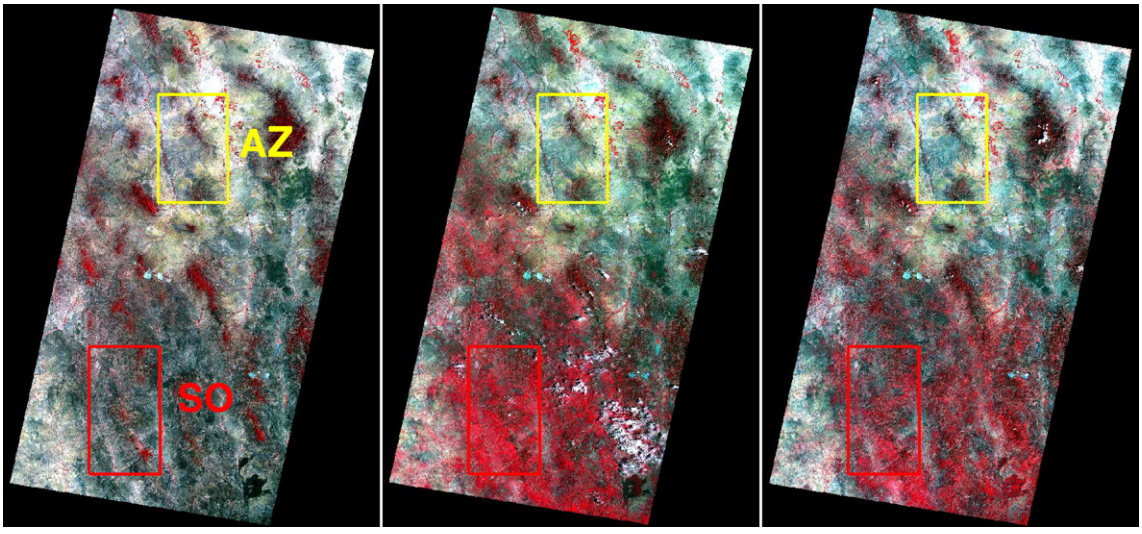

Fig. 1. False color composite (Band 4 — red, Band 3 — green, Band 2 — blue) Landsat 5 images over the SMEX04 domain on June 11, July 29 and August 30, 2004. The AZ and SO domains are marked in the images. The red areas indicate more vegetation biomass.

Table 2
Frequency characteristics of PSR/CXI channels during the SMEX04 mission

Frequency (GHz)	Frequency Band (GHz)	Polarizations	Beamwidth
6.00	5.82–6.15	v, h	10°
6.50	6.32–6.65	v, h	10°
6.92	6.75–7.10 [a]	v, h, U, V	10°
7.32	7.15–7.50	v, h	10°
10.64	10.63–10.65	v, h	7°
10.69	10.68–10.70	v, h	7°
10.70	10.6–10.8 [a]	v, h, U, V	7°
10.75	10.74–10.76	v, h	7°
Thermal	9.6–11.5 um	–	7°

[a] AMSR-E channels.

rock fragment cover (erosion pavement) can range from nearly 0% on shallow slopes to over 70% on the very steep slopes.

The WGEW is densely instrumented with rainfall recorded on a continuous basis at eighty-eight locations. Twenty-seven capacitance based soil moisture probes have been installed at twenty-one locations on or near the 150 km^2 watershed. Nineteen locations are on the watershed, all of these are co-located with electronic-measuring digital-recording rain gauges; sixteen of these have a single sensor at 5 cm depth, the other three sites have a shallow profile array of 3 sensors at 5, 15 and 30 cm. All data are recorded at 30-minute intervals and are automatically reported to a data archiving location (Cosh et al., 2008-this issue).

2.2. Sonora study region

The Sonora experimental site (SO) is located in the Rio Sonora Watershed in northern Mexico. It consists of a 50 by 90 km area that includes six EASE-Grid cells (25 × 25 km each). The vegetation is diverse and dominated by scrubland and sub-tropical vegetation (~33% each). Sub-tropical vegetation is located mainly in the south and scrubland in the north. Coniferous vegetation (20%) occurs in the mountains near the center of the SO domain. Grasslands are mixed with conifers or perennial species. Topography in the region is highly variable.

Soil moisture instruments were installed at fourteen locations distributed over a 50 by 90 km domain in the SO region. Vitel sensors were installed along with rain gauges. All sites include a 5 cm depth sensor providing both soil moisture and temperature. Data are recorded at 20-minute intervals.

Some of the regional characteristics of the AZ region apply also to the Sonora (SO). However, there is more significant topographic variation and a greater amount and mixture of vegetation within the area of Sonora that has been selected than AZ. The sub-tropical vegetation in the SO region also exhibited significant increases in biomass and vegetation water content in response to the rainfall that occurred prior to SMEX04.

2.3. SMEX04 field campaign soil moisture sampling

Ground-based observations during SMEX04 included a combination of in-situ and mobile soil moisture data collection. The in-situ portion (Cosh et al., 2008-this issue) was supplemented with more intensive ground-based sampling using traditional sampling methods on the aircraft/satellite coverage dates.

Three different sampling strategies were employed: regional, watershed, and topographic gradient. The goal of regional soil moisture sampling was to provide a reliable estimate of the volumetric soil moisture (VSM) mean and variance within a single satellite passive microwave footprint (~50 km) and multiple EASE-Grid 25 km cells concurrent (or as close as possible) with the Aqua AMSR-E overpass (1330 local standard time). For AZ, a grid of 40 sites was sampled each day over the 50 km by 75 km domain. In SO, up to 50 sites were sampled in the 50 km by 90 km domain. These measurements were used primarily to support the AMSR-E based microwave observations; therefore, the regional sampling was conducted within a +/− two-hour time window of the satellite overpass.

Regional sampling in the AZ region was complemented with more intensive watershed sampling at 64 rain gauge locations within the WG watershed. Topographic gradient sampling was conducted only in SO and consisted of a single transect of 30 points across elevation contours (Vivoni et al., 2007).

Additional details on SMEX04 can be found on the website (http://www.ars.usda.gov/research/docs.htm?docid=8995).

3. PSR/CX and aircraft mission description

Aircraft observations provide the critical bridge for scaling and integrating in-site point observations to the coarse satellite footprints. In addition, the higher resolution aircraft soil moisture products are of value in more intensive hydrologic investigations. A Naval Research Lab (NRL) aircraft (P-3B) was used in SMEX04 as host to the PSR instrument, which simulates the low frequency channels of AMSR-E.

The PSR is an airborne microwave imaging radiometer (Piepmeier & Gasiewski, 2001) developed for the purpose of obtaining polarimetric microwave emission. It has been successfully used in several major experiments including SGP99 (Jackson et al., 2002), SMEX02 (Bindlish et al., 2006), and SMEX03 (Jackson et al., 2005).

A typical PSR aircraft installation is comprised of four primary components: 1) scanhead, 2) positioner, 3) data acquisition system, and 4) software for instrument control and operation. The scanhead houses the PSR radiometers, antennas,

Table 3
PSR/CX flight line and mapping parameters during SMEX04

PSR flight line and mapping specification for SMEX04	
Altitude (m)	7300
Number of parallel flight lines	4
Flight line length (km)	75 (AZ), 90 (SO)
Flight line spacing (km)	11
Swath width (km)	19
Scan period (s)	3
Incidence angle (°)	55
3-dB footprint resolution	3.0 km at 6.925 GHz, 2.0 km at 10.7 GHz

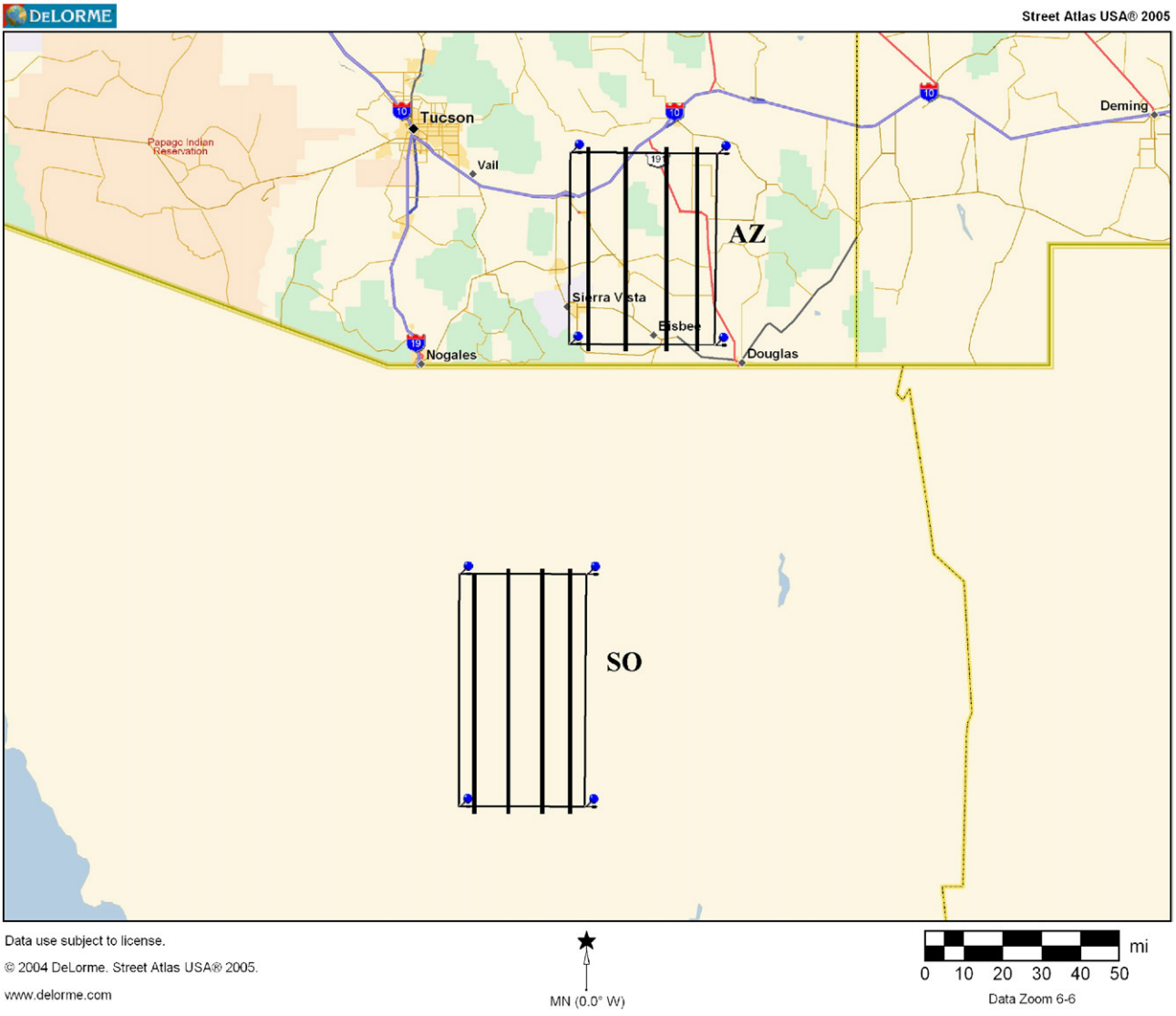

Fig. 2. Location of the two sampling domains and the flightlines over each domain.

video and IR sensors, A/D sampling system, and associated supporting electronics. The scanhead can be rotated in azimuth and elevation to any arbitrary angle. Additional details on the PSR not presented here can be found at http://cet.colorado.edu/.

During SMEX04, the PSR/CX scanhead was integrated onto the P-3 aircraft in the aft portion of the bomb bay. The PSR/CX system provided horizontal (H) and vertical polarization (V) measurements within four adjacent frequency sub-bands in both C- and X-bands (Table 2). The multi-band capability of PSR/CX facilitates the investigation of using frequency agile radiometry for observations over interference prone regions. For SMEX04, the system operated in a conically scanned imaging mode with a 55° incidence angle. PSR and flight line characteristics that are significant for the mapping mission design are listed in Table 3. The intensive observing period was August 5–August 26, 2004 (Table 1). The flight lines over the two domains are shown in Fig. 2. Note that the SO sampling domain was 50 km × 90 km as compared to the AZ sampling domain of 50 km × 75 km in order to include an in-situ site located in the southern portion.

The P3-B flights had to be biased somewhat earlier than the AMSR-E overpass time to avoid flights disruptions due to

Table 4
PSR flight times (local times) over the SO and AZ domains

Date (August 2004)	SO	AZ
5	15:14–16:01	16:27–16:55
7	11:35–12:40	–
8	9:38–10:14	10:58–11:41
9	9:23–10:11	10:33–11:33
10	9:19–10:06	10:33–11:12
12	9:36–10:26	10:57–11:37
13	9:37–10:24	10:44–11:24
14	9:36–10:25	–
24	9:46–10:32	10:58–11:39
25	13:11–14:00	14:53–15:32
26	9:36–11:17	12:18–12:58, 13:03–13:49

Table 5
Percentage of PSR observed pixels contaminated with RFI at C-band over the AZ domain for the four PSR sub-bands

Date	6.92 V GHz (%)	6.92 H GHz (%)	7.32 V GHz (%)	7.32 H GHz (%)
Aug 5	50	44	40	28
Aug 8	52	44	27	19
Aug 9	60	55	32	20
Aug 10	54	44	32	19
Aug 12	63	54	25	17
Aug 13	54	52	22	18
Aug 24	56	55	27	18
Aug 25	55	49	27	13
Aug 26	60	61	25	18

thunderstorms. This restriction resulted in non-concurrent measurements between aircraft and satellite overpasses. The daily mission duration was limited to no more than 4 hours. The PSR flight times are listed in Table 4. The difference in aircraft and satellite overpass times will be discussed later in the validation section.

3.1. RFI mitigation

An initial review of the PSR/CX data for all the C-band frequencies available indicated that anthropogenic radio frequency interference (RFI) was present in all channels and both polarizations, although generally not simultaneously. RFI is manifested by higher than expected brightness temperatures (T_B), sometimes exceeding the nominal geophysical brightness temperatures by hundreds of Kelvin. In most cases the RFI was spatially localized, temporally consistent from day to day, and often sometimes observed in all channels simultaneously.

One purpose of using multiple sub-bands for each primary PSR/CX band is to provide a means of detecting anthropogenic radio frequency interference. Such an interference detection and correction algorithm was successfully demonstrated using PSR data from the 1999 Southern Great Plains Experiment (SGP99) (Gasiewski et al., 2002). The algorithm compares brightness temperatures in several nearby sub-bands through the use of a standard spectral model.

As anticipated, interference was also observed during the SMEX04 experiment over the AZ domain, particularly in the AMSR-E 6.925 GHz band. The PSR/CX sub-bands were used to identify the general location of the interference and to select the frequency band with the least contamination. Table 5 shows the number of pixels detected as RFI contaminated over the AZ domain. In the AZ domain, 20% of the pixels were contaminated with RFI for the 7.32 GHz band (50% of the observations were contaminated with RFI at 6.92 GHz). The C-band observations over the SO area showed RFI contamination for less than 5% of the pixels. This pattern was consistent throughout the SMEX04 campaign. RFI locations were typically independent of time. The SMEX04 RFI patterns are consistent with the results presented by Li et al. (2004), which showed significant amounts of RFI at 6.925 GHz over the continental U.S. Relatively few occurrences of interference were observed at X-band. Based upon a close examination of the RFI in the data, we concluded that the 7.32 GHz and 10.7 GHz bands were far superior to the others. Therefore, all further analyses consider only these channels.

3.2. Temporal normalization

Collecting high resolution radiometric data over a large region requires considerable aircraft flight time. For SMEX04, it took ~4 hours to complete a mapping sequence on any given day (~1 hour for each sampling domain, plus transit time). During this time interval, both the brightness temperature and physical temperature increased over the course of the flight. Long-term drifts in instrument characteristics not accounted for in the calibration process also caused some brightness temperature variations over the flight period. Since we wished to have the equivalent of an instantaneous snapshot of the region, it was necessary to normalize the observed imagery to a single instant of time.

By design, the data from any given flight line overlapped the data from adjacent flight lines by ~9% of the area of each swath. It is assumed that no temporal correction was needed within a given flight line, but rather only from line to line. In addition, the second of each of the four north–south lines on each day was used as a standard for that day. Following the above assumptions, all data points in the overlapping areas of the flight lines were identified and averaged by line. The average of this area for each line was compared to the same area for each adjacent line and line 2 to determine a correction offset. This technique has been employed in previous aircraft missions (Bindlish et al., 2006; Jackson et al., 2002, 2005).

4. AMSR-E and PSR brightness temperature intercomparison

One of the goals of SMEX04 was to provide a validation over land of the brightness temperature products generated from the Aqua AMSR-E sensor. Concurrent satellite and aircraft observations were available on 8 days (August 5, 7, 9, 10, 12, 14, 25 and 26) (Table 1). For these days the PSR

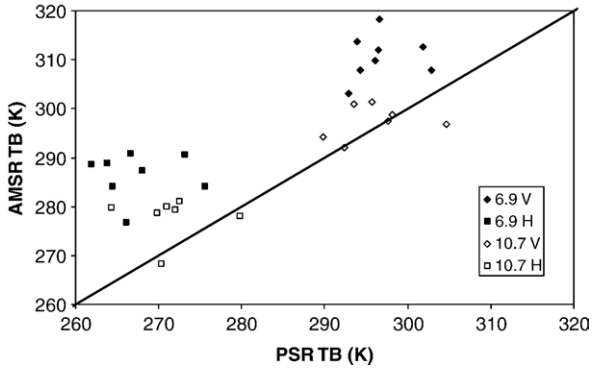

Fig. 3. Comparison between the PSR and AMSR-E observed brightness over the AZ domain for the C-band and X-band frequencies at both horizontal (H) and vertical (V) polarizations.

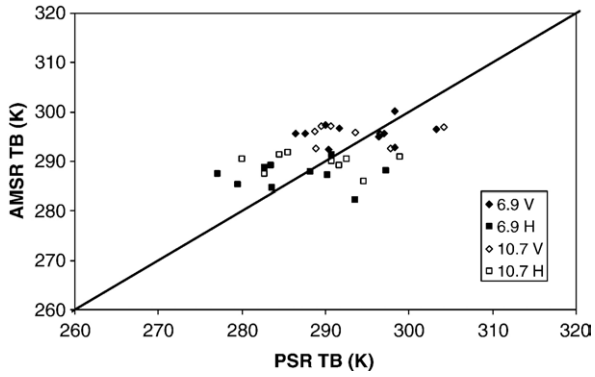

Fig. 4. Comparison between the PSR and AMSR-E observed brightness over the SO domain for the C-band and X-band frequencies at both horizontal (H) and vertical (V) polarizations.

brightness temperature (T_B) observations at 7.32 and 10.7 GHz for both vertical and horizontal polarizations were averaged over each regional domain (~80,000 PSR footprints). Average AMSR-E T_B values were also computed for both the 6.925 GHz and 10.7 GHz frequency channels. The results (Figs. 3 and 4) indicate that the AMSR-E T_B and PSR T_B at X-band for both V and H polarizations are nominally the same. The AMSR-E C-band channels are warmer than expected over the AZ domain by ~15–20 K. As mentioned earlier, the PSR flights were flown earlier during the day, thus potentially resulting in somewhat lower brightness temperatures due to lower surface temperatures. However, if this was a major effect it would be observed for both C-and X-band and in both the AZ and SO domains. The brightness temperatures for the SO domain agree well with the AMSR-E observations at both C-and X-band. Thus, we ruled out temporal sampling error as a source of this difference.

The PSR brightness temperatures for the SO domain agree well with the AMSR-E observations for both C- and X-band. This indicates a good calibration of the AMSR-E channels in this T_B range, assuming that the PSR was well calibrated during the SMEX04 campaign. The dynamic range of the PSR brightness temperatures is larger than that of the AMSR-E observations. The brightness temperature results indicated no bias between the two platforms. The agreement between the average of the coarse resolution AMSR-E observations and high resolution PSR observations at X-band also supports the assumption that scaling of brightness temperature in this domain is linear. High resolution PSR observations allow the possibility to study the small scale soil moisture variations.

The C-band results clearly indicate a significant bias (AMSR-E > PSR), due to the presence of RFI (Fig. 3). By analyzing the PSR multiple sub-band channels, it was determined that the AMSR-E 6.9 GHz data for the AZ domain contained RFI contamination, whereas the aircraft data at 7.32 GHz had only

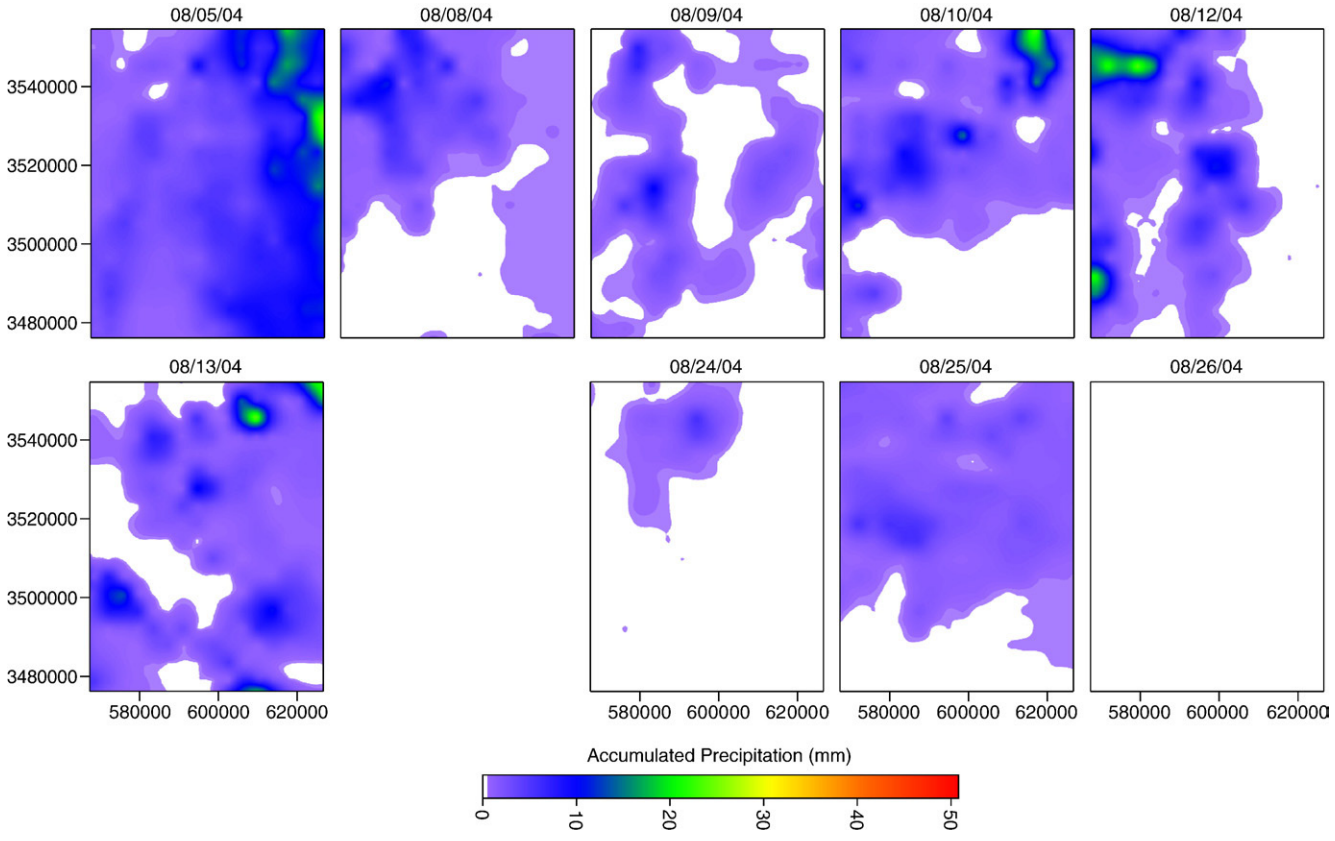

Fig. 5. Spatial distribution of the radar estimated daily precipitation accumulations over the AZ domain. Precipitation accumulations are for 24 h prior to the PSR observations. The precipitation accumulations were re-projected in UTM coordinates (zone 12).

minor contamination. The SMEX04 sampling domain included areas with and without the presence of significant RFI. The change in observed T_B at these frequencies on different dates is due to changes in areas not affected by RFI. The change in geophysical response over the C-band (6.5 GHz–7.3 GHz) is small and is within the noise levels of the instrument. The presence of multiple sub-bands in PSR/CX at C-band provided an opportunity to develop mitigation measures against RFI. The presence of RFI in C-band AMSR-E observations raises questions about the reliability of soil moisture estimates made using these observations.

5. Soil moisture algorithm

The relationships between brightness temperature (T_B) and soil moisture, surface roughness and vegetation water content are nonlinear. The algorithm for deriving soil moisture and temperature from T_B observations used here is similar to that described in Jackson (1993) and is based on physical models of microwave emission from a layered soil–vegetation–atmosphere medium. Atmospheric effects were assumed to be minimal for this study. Surface emissivity (e_s) is calculated by dividing the brightness temperature by the soil surface temperature (T_S). The pixel emissivity is corrected for vegetation using the approach described in Jackson and Schmugge (1991). In this approach the vegetation is treated as an attenuating layer with transmissivity (γ) that depends on the vegetation optical depth (τ) and the incidence angle (θ). The soil is represented as a semi-infinite soil layer of effective physical temperature T_e, an air–soil reflectivity r, with a layer of vegetation of physical temperature ($T_e = T_c$). The resulting equations used are:

$$T_B = eT_e\exp(-\tau) + T_c(1-\alpha)[1-\exp(-\tau)] \times [1 + r\exp(-\tau)] \quad (1)$$

$$\gamma^2 = \exp[-2\tau(\sec\theta)] \quad (2)$$

where e and r are the emissivity and reflectivity of the soil surface and α is the single scattering albedo of vegetation. The optical depth of the canopy is determined using a first-order approximation of the vegetation parameter (b), which is a function of land use, and vegetation water content (VWC). A constant value of $b = 0.3$ was used in the retrieval process. The effect of surface roughness (s) on soil reflectivity (r') can be

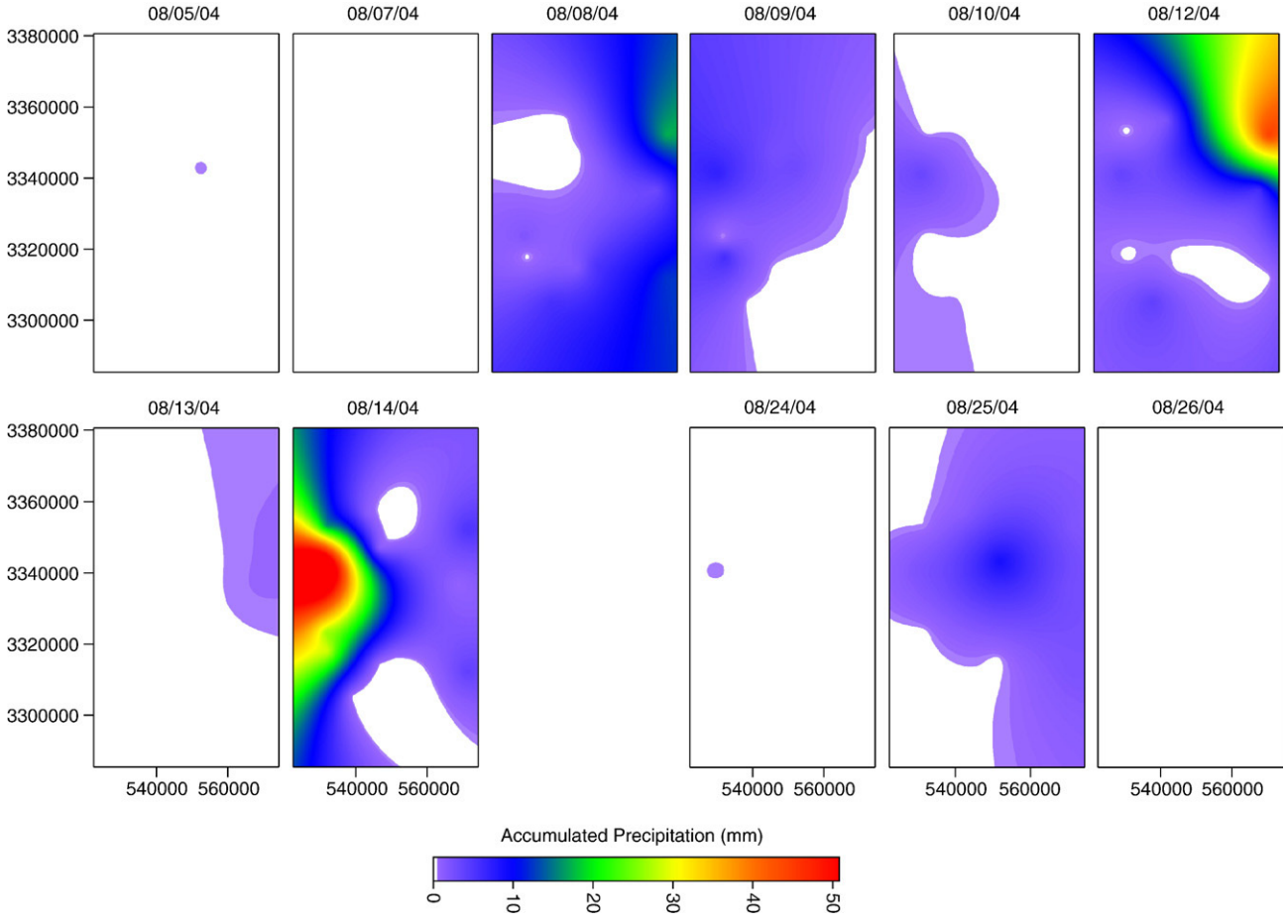

Fig. 6. Spatial distribution of the rain gauge based daily precipitation accumulations over the SO domain. Gauge observed precipitation observations were gridded in UTM coordinates (zone 12) using kriging.

characterized using the relationship described in Choudhury et al. (1979). The roughness parameter was assumed to be a function of landuse sub-domains (see Section 6). The roughness parameter was optimized using PSR observations for all the days. Optimization was performed to maximize the number of PSR retrievals with physically acceptable dielectric constant estimates (between rock and water). No soil moisture observations were used in the optimization process. A 3×3 mean filter (spatial resolution of 2.4 km) was used over this discrete roughness parameterization (3 dB footprint of PSR is 3.0 km). Finally, the dielectric mixing model (Wang & Schmugge, 1980), which is based on soil texture, was used to estimate volumetric soil moisture at each pixel.

The algorithm requires several ancillary data sets for implementation: surface soil texture, land cover, and Normalized Difference Vegetation Index (NDVI) for VWC estimation. The following summarizes the decisions and datasets selected for this process.

5.1. Surface soil texture

Soil properties do not usually change quickly and, therefore, this plane of ancillary data is considered constant in time. A multi-layer soil characteristics data set for the state of Arizona developed by SSURGO was adapted for this work.

5.2. Soil temperature

Soil temperature measurements at 1 cm, 5 cm, and 10 cm were made at all the sampling sites during the experiment. The 5 cm measurements were interpolated at the mapping resolution.

5.3. Land cover and vegetation water content

Land cover over the mapping domain was determined using Landsat imagery (Yilmaz et al., 2006). Vegetation water content was estimated using the high resolution Landsat imagery on a weekly basis. These weekly values were interpolated to obtain daily estimates of VWC (Yilmaz et al., 2006).

6. Brightness temperature and soil moisture mapping

There was significantly higher precipitation during the first half of the experiment than the second half. Very little precipitation occurred in the sampling domain after August 17, 2004. Fig. 5 shows the radar estimated precipitation accumulations for the 24-hour period prior to P3 flights over the AZ sampling domain. The AZ domain receives good coverage from the NOAA/NWS WSR-88D Doppler weather radar. The only rain gauges in the AZ regional domain that were applicable to this investigation were those located in the Walnut

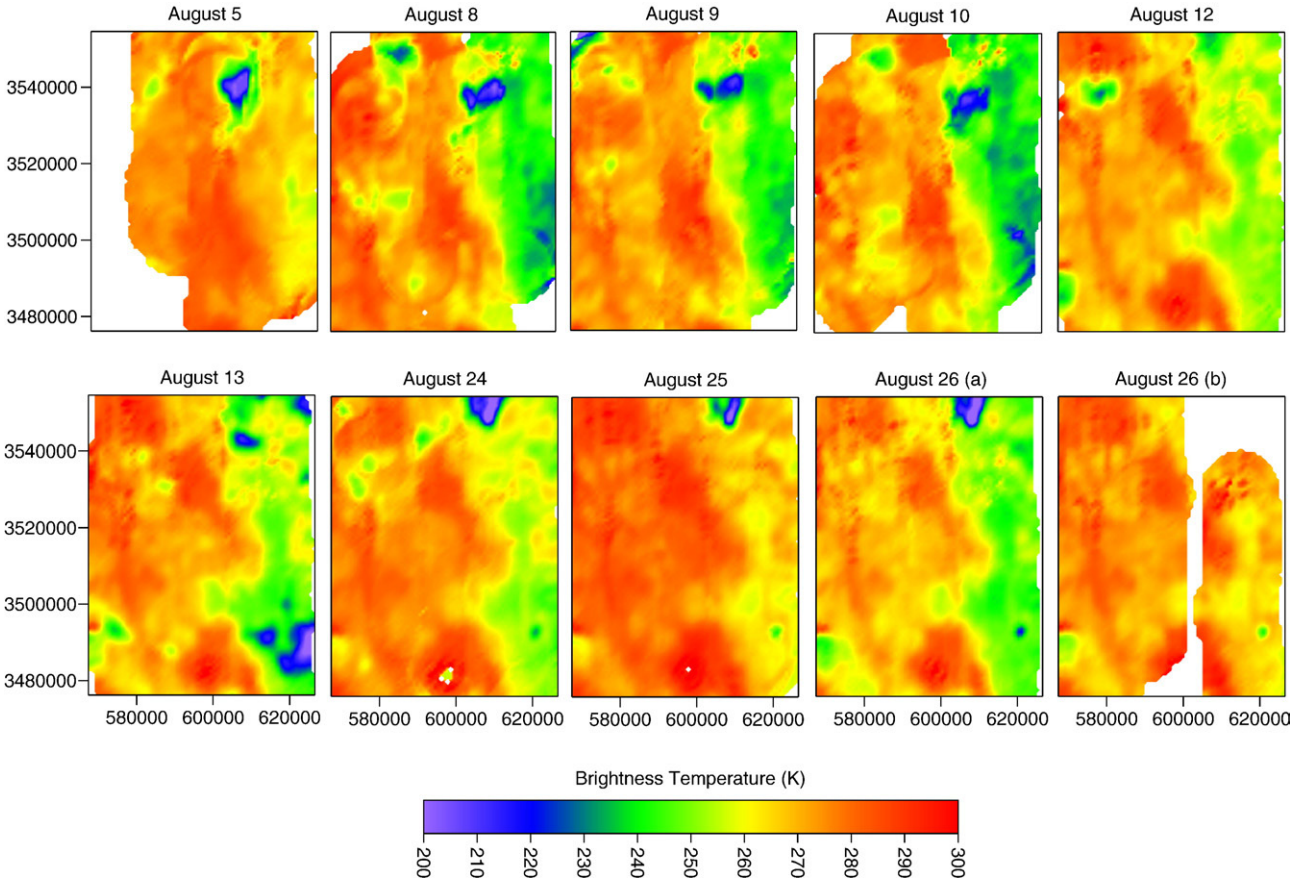

Fig. 7. PSR observed brightness temperatures at 7.32 H GHz over the AZ domain.

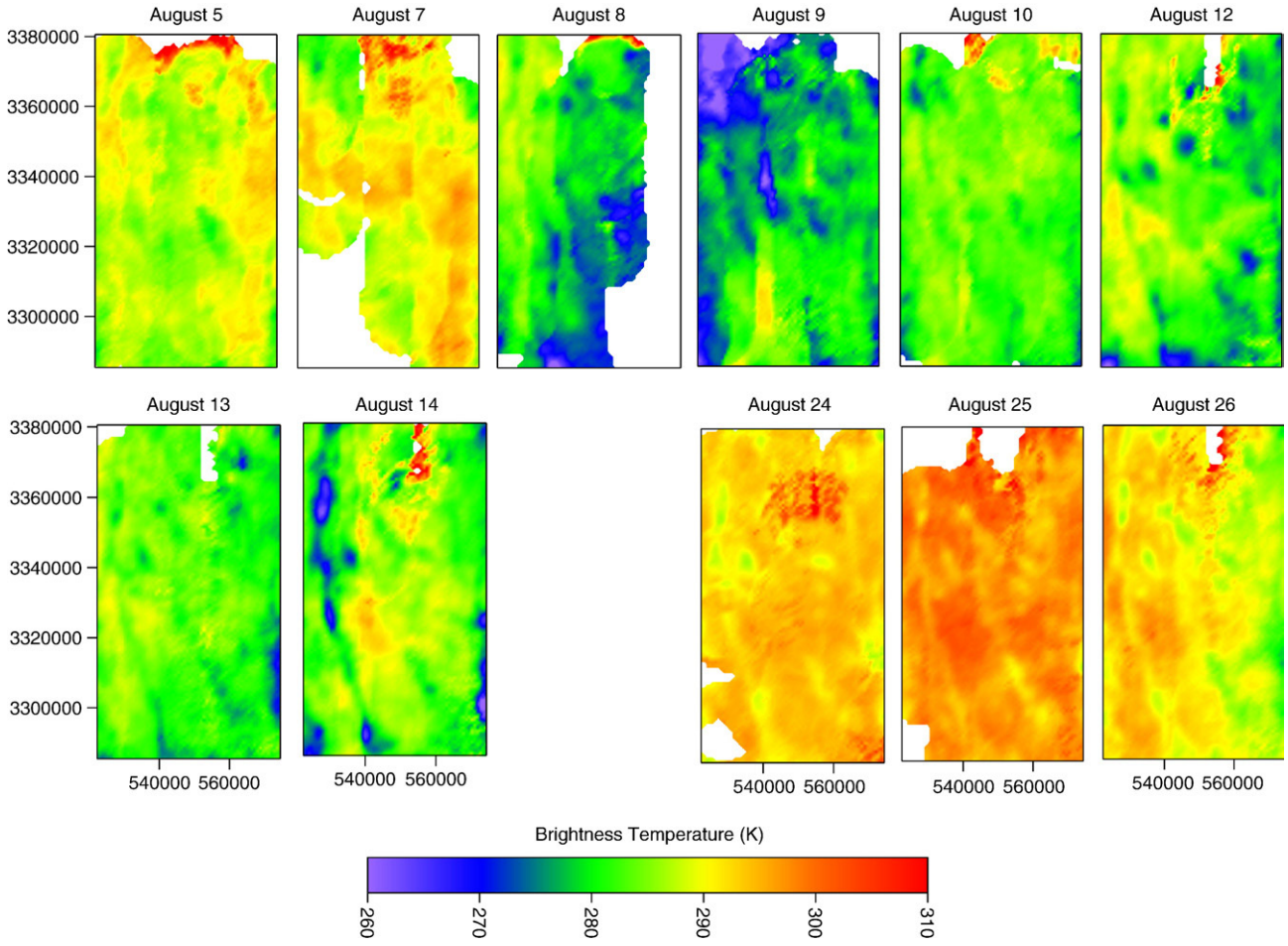

Fig. 8. PSR observed brightness temperatures at 7.32 H GHz over the SO domain.

Gulch watershed. There was no Doppler radar coverage in the SO domain. To mitigate this lack of precipitation data, 13 rain gauges were co-located with the in-situ soil moisture network in the SO domain. Point rain gauge observed daily precipitation accumulations were gridded to map the spatial distribution over the SO domain (Fig. 6).

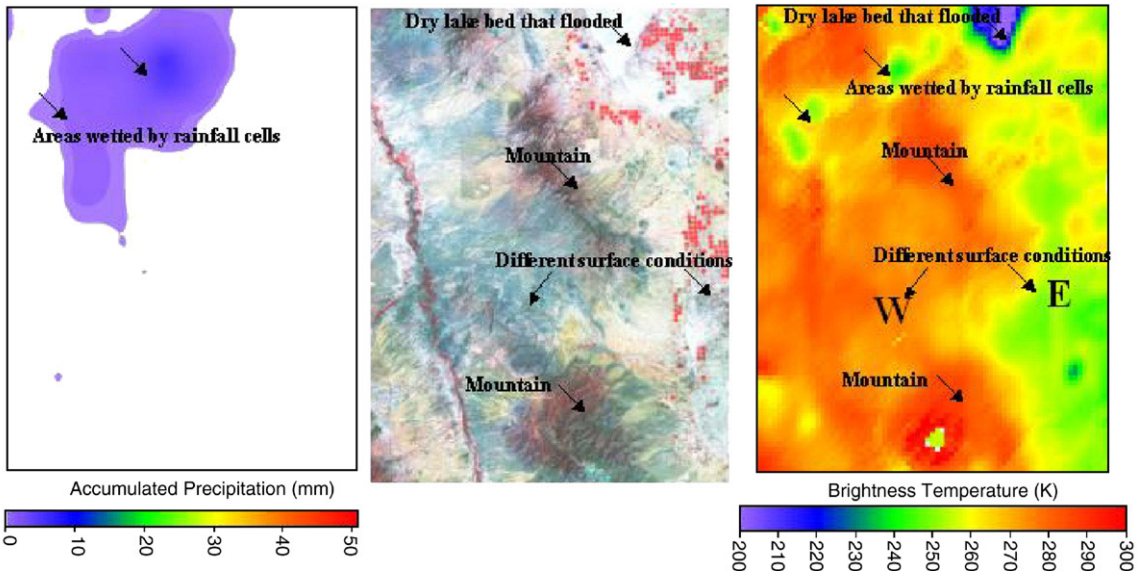

Fig. 9. Features of the PSR observations for August 24, 2004 over the AZ domain. (a) 24-hour precipitation accumulation prior to the PSR flight on August 24, (b) Landsat 5 image over the AZ domain on July 29, 2004, and (c) PSR observed brightness temperature at 7.32 H GHz.

Fig. 10. Picture of the flooding event in the San Maguel river valley on August 14, 2004.

Brightness temperature observations were processed as described in a previous section of this paper to produce brightness temperature images on a fixed grid over the study area. PSR based images at H-polarization C-band (7.32 H GHz) for each day are presented in Fig. 7 for AZ and Fig. 8 for SO. The SO domain had much higher amounts of vegetation than the AZ domain, which resulted in higher brightness temperature observations throughout SO. Vegetation also contributes to the smaller dynamic range of brightness temperature observations. Consistent spatial structure and temporal patterns from day-to-day were apparent in both regions. The range of brightness temperatures in the two regions is very different and is highly dependent on the surface features. These images (Figs. 7 and 8) should be interpreted with reference to Figs. 1, 5 and 6). Fig. 9 shows the 24 h accumulated precipitation prior to the August 24 P3-B flight, the brightness temperature image for August 24, 2004 and the Landsat imagery over the AZ sampling domain. The Wilcox Playa (a dry lake — located in the northeast corner of the AZ domain) was flooded with water as the result of heavy precipitation on August 14, 2004. Consequently, the dry lake exhibited a much lower brightness temperature than the surrounding areas. The northern part of the domain received some precipitation, which resulted in lower brightness temperatures over that area. The two mountain areas (Cochise and Mull mountains) have a significant amount of exposed rock. The presence of rock results in higher brightness temperature observations over these areas. The western part of the domain had higher rock contents than the eastern side. The eastern side is flatter and has a higher sand content than the western side. Also, there are a few irrigated fields in the northeast part of the domain. These conditions resulted in generally higher brightness temperature observations on the western part of the AZ domain versus the eastern part. These brightness temperature trends were consistent throughout the duration of the experiment.

Fig. 10 shows the flooded Rio San Miguel in the SO domain on August 14, 2004. This flooding can also be observed in the brightness temperature images for that day. Fig. 11 shows the brightness temperature images for August 13 and 14, accumulated precipitation prior to August 14 and the Landsat image over the SO domain. The river valley and the area that received heavy precipitation show significantly lower brightness temperatures on August 14 (10–15 K lower than on August 13). The increase in soil moisture is apparent despite the fact that the SO domain had greater amounts of vegetation resulting in a smaller brightness temperature dynamic range than the AZ domain. Higher brightness temperatures associated with the dryer mountain areas can also be seen within the SO domain.

Brightness temperature observations were used in the single channel soil moisture retrieval algorithm to estimate volumetric soil moisture over the AZ domain (Fig. 12). The resulting VSM estimates are generally consistent with the brightness temperature observations. The eastern part of the AZ domain is always wetter than the western side. The AZ domain is dominated by very sandy soil with sparse vegetation, which results in very high infiltration rates. The soils in this area do not retain the moisture over long periods of time. After a precipitation event, drydown over this domain occurs over a period of approximately 24 hours. The range of soil moisture observed was thus lower (<0.20 m^3/m^3) than for most regions after precipitation. The Wilcox Playa dry lake was inundated with water on August 24–26, which can be seen in the soil moisture maps. The entire AZ domain became very dry (~ 0.05 m^3/m^3 areal average) towards the end of the experiment.

The average of the PSR estimated soil moisture over the AZ domain was compared to the average of the in-situ soil moisture

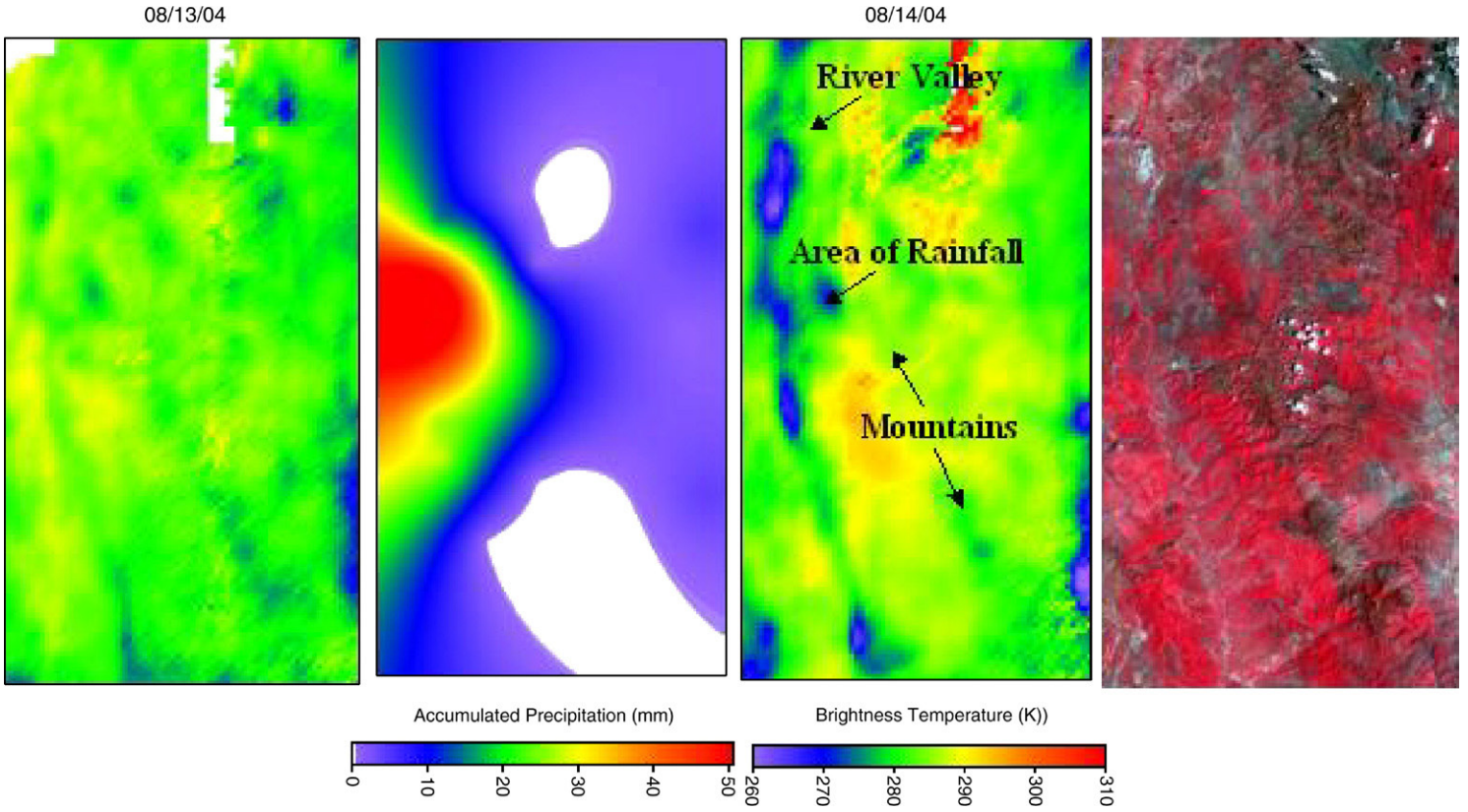

Fig. 11. Features of the PSR observations for August 14, 2004 over SO domain. (a) PSR observed brightness temperature at 7.32 H GHz on August 13, (b) 24-hour precipitation accumulation prior to the PSR flight on August 14, (c) PSR observed brightness temperature at 7.32 H GHz on August 14, and (d) Landsat 5 image over the AZ domain on July 29, 2004.

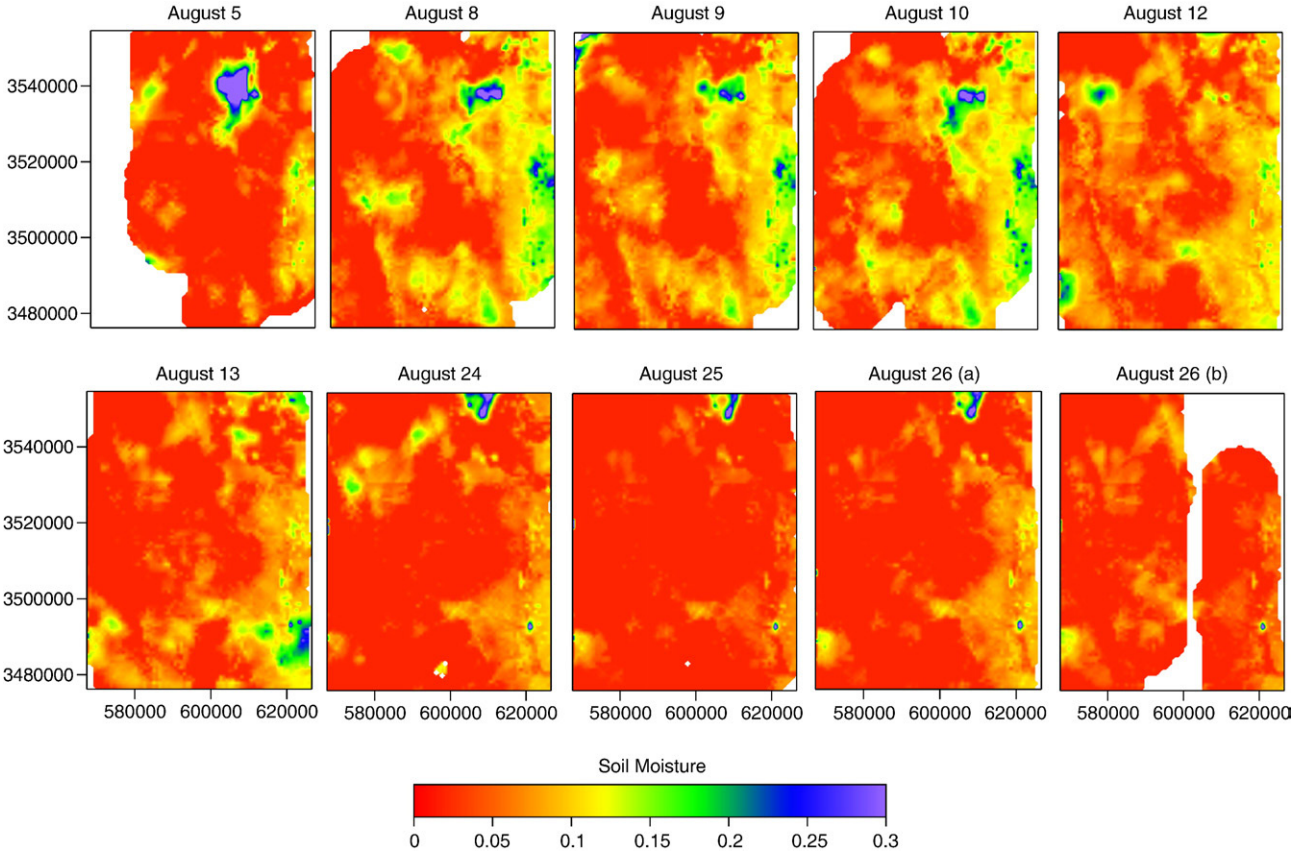

Fig. 12. PSR estimated soil moisture over the AZ domain.

measurements (Fig. 13). The results compared well with the observations, exhibiting a standard estimate of error (SEE) of 0.014 cm^3/cm^3. The PSR estimated soil moisture exhibited no significant bias. To investigate the effect of landuse on soil moisture retrieval, the AZ domain was divided into different physical sub-domains based on landuse classification, elevation and size of the sub-domain (Fig. 14). A Digital Elevation Model (DEM) was used to sub-divide the Mule Mountain, Cochise Mountain and northern mountain areas. Landuse was also used to separate the agricultural and the riparian zones. The Walnut Gulch watershed was considered a single unit, and the rangelands on the east and west were each divided into two parts. Fig. 14 shows the locations of the sampling sites along with the various sub-domains. The average of the PSR estimated soil moisture over these sub-domains was compared to the average in-situ soil moisture observations (Fig. 15). The comparison over the northern mountains was eliminated since this sub-domain contained only one soil moisture sampling location. Comparison of the soil moisture values shows a significantly higher amount of scatter than the domain average comparison in Fig. 13. No significant bias was found for any of the sub-domains. The SEE for each sub-domain ranges from 0.025 cm^3/cm^3 to 0.041 cm^3/cm^3. Considering, the range of observed soil moisture observations (0.0–0.13 cm^3/cm^3) the errors in estimated soil moisture are significant. The overall SEE for the sub-domain based comparison was 0.032 cm^3/cm^3 as compared to the in-situ observation. This represents 25% of the observed range of observed soil moisture observations. As the soil moisture decreases the relative contribution of soil moisture to the microwave signal decreases.

The single-channel soil moisture algorithm was also applied to PSR observations over the SO domain (Fig. 16). Again, the estimated soil moisture values are consistent with the brightness temperature patterns. However, the soil moisture over the SO domain has a larger dynamic range than the AZ domain. The southern part of the SO domain was typically wetter than the

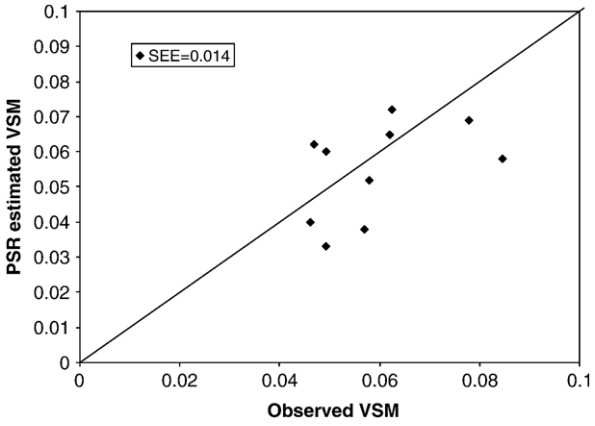

Fig. 13. Comparison of PSR estimated soil moisture with observed measurements over the entire AZ sampling domain.

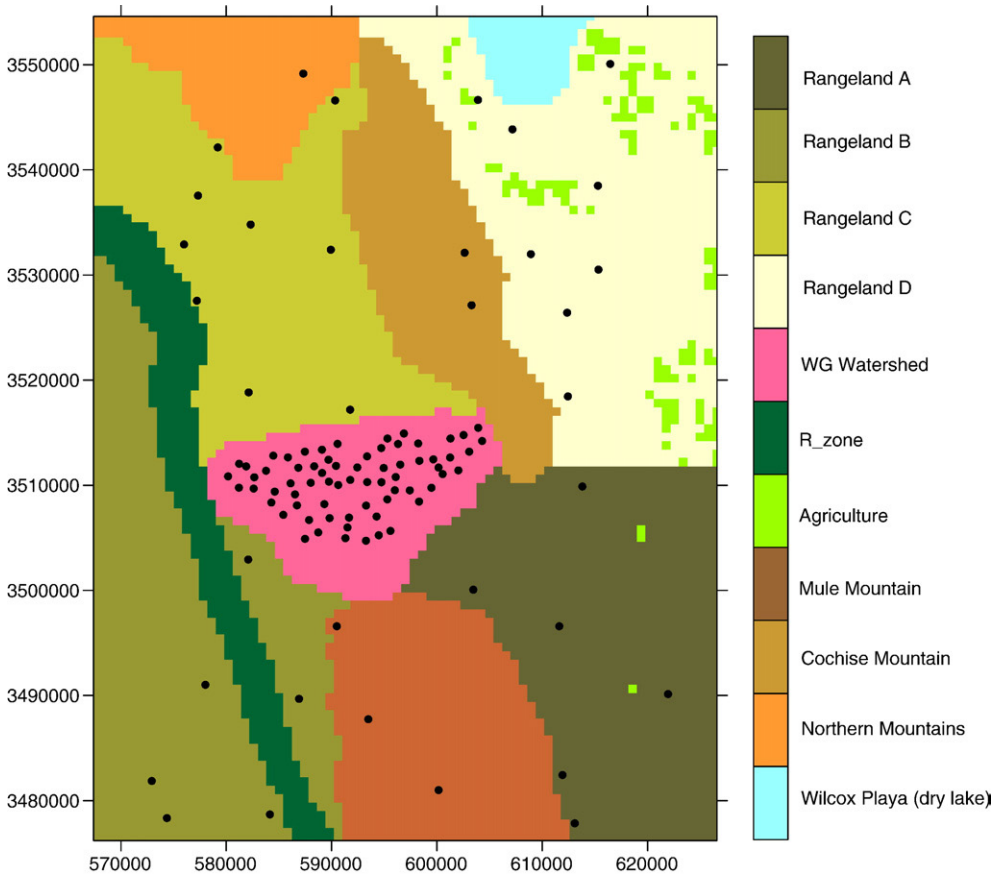

Fig. 14. Landuse based sub-domain in the AZ region. The black points represent the soil moisture ground sampling locations.

northern half as might be expected since, the NAMS originates in the south and tracks northward up the SMEX04 domain. This could result in higher soil moisture estimates in the southern domain. The Rio San Miguel river valley can easily be seen in the soil moisture images. This drains from North to South, also contributed to the soil moisture pattern. On August 14, 2004 the soil moisture estimates over the Rio San Miguel river valley are particularly high (>0.30 m^3/m^3), as previously discussed. The high soil moisture indicates saturated soil moisture conditions consistent with the observed flooding in the Rio San Miguel river valley.

The average of the PSR estimated soil moisture over the SO domain was compared to the average of the ground-based observed soil moisture measurements (Fig. 17). The results compared well with the observations (SEE = 0.021 cm^3/cm^3), which is slightly higher than that found for the AZ domain. This increase in error is not unexpected considering the increase in vegetation water content and topographic variability in SO. Again, the PSR estimated soil moisture exhibits no significant bias with respect to in-situ observations.

7. Summary

The Soil Moisture Experiment 2004 (SMEX04) was designed to address critical issues regarding the design of future satellite-based soil moisture missions and the exploitation of the currently available systems. Equally important was the provision of spatial soil moisture information to support the NAME related investigations of land-atmosphere interaction.

While the overall scientific value of the SMEX04 data set was impacted by the lack of rainfall during the campaign and the problems with the performance of the aircraft platform, the data that was obtained was of high quality and was useful for studying the effects of land surface variations and rugged topography on soil moisture retrieval. Precipitation was more

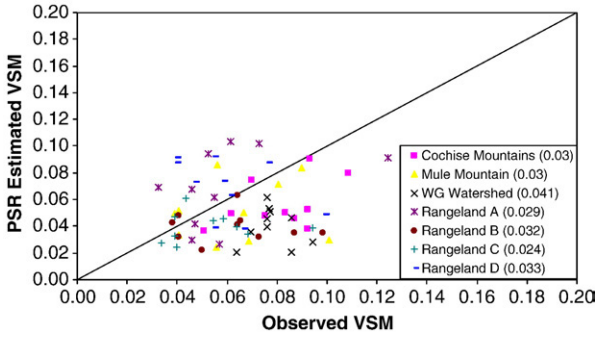

Fig. 15. Comparison of PSR estimated soil moisture with observed measurements over the different sub-domains in the AZ region. The numbers in parenthesis represent the SEE for the corresponding sub-domain. The overall SEE for all the sub-domains was 0.032 cm^3/cm^3.

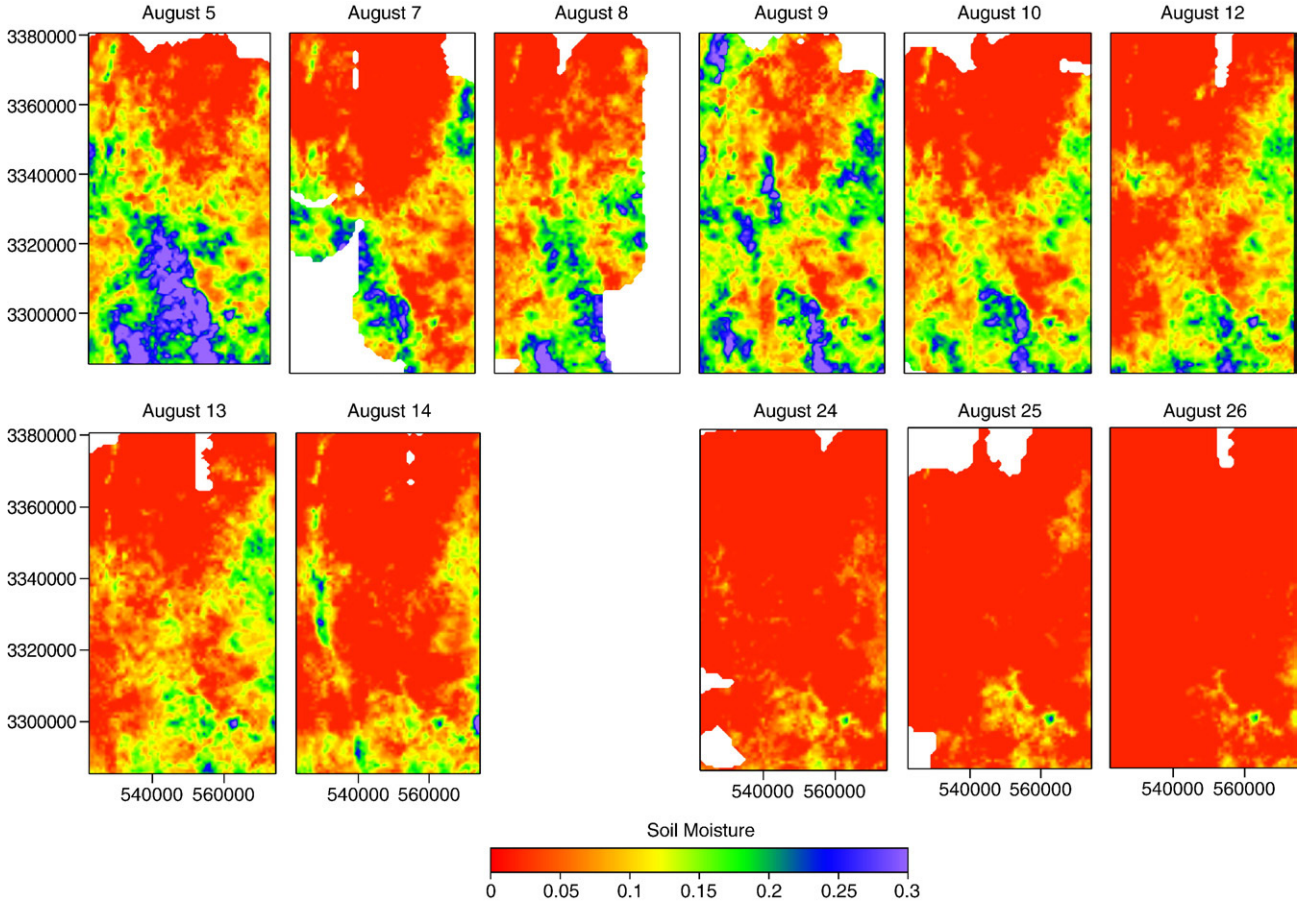

Fig. 16. PSR estimated soil moisture over the SO sampling domain.

widespread and higher in SO than AZ during the SMEX04 experiment, which also had higher amounts of vegetation biomass and topographic variability.

A significant result of the analysis was that the PSR and AMSR-E brightness temperature observations were consistent at both C-and X-band frequencies over the SO domain. Over the AZ domain, the brightness temperatures were consistent at X-band frequencies, but the AMSR-E observations were higher than the PSR observation at C-band. The differences can be attributed to the presence of RFI in AMSR-E observations at C-band over the AZ domain. This consistency supports the conclusion that both instruments are adequately calibrated for land studies.

Spatial distributions of the PSR observed brightness temperatures were consistent with geophysical features and spatial patterns of accumulated precipitation. PSR estimated soil moistures were in agreement with the in-situ ground-based observed soil moisture. The estimated error was higher over the SO domain (SEE = 0.021 cm^3/cm^3) than the AZ domain (SEE = 0.014 cm^3/cm^3). These results show that it is possibility possible to retrieve soil moisture in areas of moderate vegetation biomass and high topographic variability at aircraft spatial resolutions. PSR observations did not show any significant topographic effect at a resolution of 3.0 km. It is likely that the terrain effects in this area are minimized at these resolutions. The presence of rocks (resulting in higher surface roughness) and vegetation minimizes the effect of incidence angle of observed brightness temperature. It is possible a facet based micro-model may show the significance of topographic variations. It is likely the sub-pixels are oriented in opposite directions and the effect on brightness temperature is cancelled. A more in-depth study that studies the sub-pixel behavior at finer resolutions maybe needed to fully understand the effect of topography.

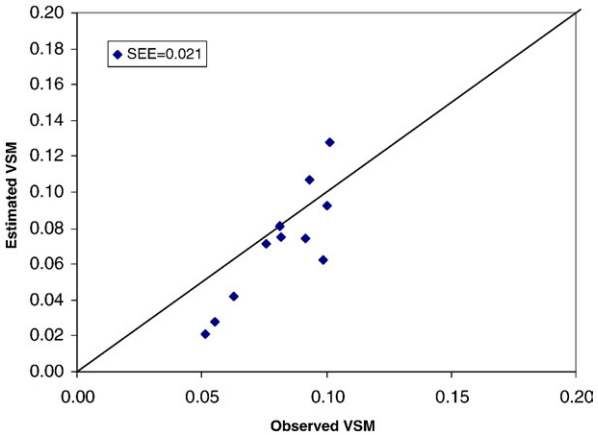

Fig. 17. Comparison of PSR estimated soil moisture with observed measurements over the entire SO sampling domain.

The PSR based soil moisture products will provide an excellent resource for the study of the effects of land surface (soil moisture in particular) on the North American Monsoon System. It is anticipated, that the SMEX04 data will provide valuable input parameters for coupled land-atmosphere models used to investigate the importance of surface parameterization. High resolution soil moisture estimates also, provide an opportunity to study the effect of spatial variability of soil moisture on atmospheric circulation. The importance of soil moisture in a convective meteorological system can be investigated. Results from PSR can be extrapolated to AMSR-E spatial scales to study a larger domain.

Acknowledgements

This work was supported by the National Aeronautics and Space Administration (NASA) EOS AMSR Instrument Science Program, NASA Terrestrial Hydrology Program and the Aqua AMSR Science Program.

References

Barlow, M., Nigam, S., & Berbery, E. H. (1998). Evolution of the North American Monsoon System. *Journal of Climate*, *11*, 2238−2257.

Bindlish, R., Jackson, T. J., Gasiewski, A. J., Klein, M., & Njoku, E. G. (2006). Soil moisture mapping and AMSR-E validation using the PSR in SMEX02. *Remote Sensing of Environment*, *103*, 127−139.

Choudhury, B. J., Schmugge, T. J., Chang, A., & Newton, R. W. (1979). Effect of surface roughness on the microwave emission from soils. *Journal of Geophysical Research*, *84*, 5699−5706.

Cosh, M. H., Jackson, T. J., Moran, S., & Bindlish, R., 2008. Temporal persistence and stability of surface soil moisture in a semi-arid watershed. *Remote Sensing of Environment*, *112*, 304−313 (this issue), doi:10.1016/j.rse.2007.07.001.

Gasiewski, A. J., Klein, M., Yevgrafov, A., & Leuskiy, V. (2002). Interference mitigation in passive microwave radiometry. *Proceeding Int. Geoscience and Remote Sensing Symp., Toronto, CA*.

Higgins, W., Ahijevych, D., Amador, J., Barros, A., Berbery, E. H., Caetano, E., et al. (2006). The NAME 2004 field campaign and modeling strategy. *Bulletin of the American Meteorological Society*, *87*, 79−94.

Jackson, T. J. (1993). Measuring surface soil moisture using passive microwave remote sensing. *Hydrological Processes*, *7*, 139−152.

Jackson, T. J., Bindlish, R., Gasiewski, A. J., Stankov, B., Klein, M., Njoku, E. G., et al. (2005). Polarimetric Scanning Radiometer C and X-band microwave observations during SMEX03. *IEEE Transactions on Geoscience and Remote Sensing*, *43*, 2418−2430.

Jackson, T. J., Gasiewski, A. J., Oldak, A., Klein, M., Njoku, E. G., Yevgrafov, A., et al. (2002). Soil moisture retrieval using the C-Band polarimetric scanning radiometer during the Southern Great Plains 1999 experiment. *IEEE Transactions on Geoscience and Remote Sensing*, *40*, 2151−2161.

Jackson, T. J., & Schmugge, T. J. (1991). Vegetation effects on the passive microwave emission of soils. *Remote Sensing of Environment*, *36*, 203−212.

Koike, T., Njoku, E. G., Jackson, T. J., & Paloscia, S. (2000). Soil moisture algorithm development and validation for the ADEOS-II/AMSR. *Proceedings of the Int. Geoscience and Remote Sensing Symposium IEEE Catalog No. 00CH37120*, *vol. III* (pp. 1253−1255).

Li, L., Njoku, E. G., Im, E., Chang, P., & St. Germain, K. (2004). A preliminary survey of radio-frequency interference over the U.S. in Aqua AMSR-E data. *IEEE Transactions on Geoscience and Remote Sensing*, *42*, 380−390.

Njoku, E. G., Jackson, T. J., Lakshmi, V., Chan, T. K., & Nghiem, S. V. (2003). Soil moisture retrieval from AMSR-E. *IEEE Transactions on Geoscience and Remote Sensing*, *41*, 215−229.

Njoku, E. G., & Li, L. (1999). Retrieval of land surface parameters using passive microwave measurements at 6 to 18 GHz. *IEEE Transactions on Geoscience and Remote Sensing*, *37*, 79−93.

Paloscia, S., Macelloni, G., Santi, E., & Koike, T. (2001). A multifrequency algorithm for the retrieval of soil moisture on a large scale using microwave data from SMMR and SSM/I satellites. *IEEE Transactions on Geoscience and Remote Sensing*, *39*, 1697−1707.

Piepmeier, J. R., & Gasiewski, A. J. (2001). High-resolution passive microwave polarimetric mapping of ocean surface wind vector fields. *IEEE Transactions on Geoscience and Remote Sensing*, *39*, 606−622.

Vivoni, E. R., Gutierrez-Jurado, H. A., Aragon, C. A., Mendez-Barroso, L. A., Rinehart, A. J., Wyckoff, R. L., et al. (2007). Variation of hydrometeorological conditions along a topographic transect in northwestern Mexico during the North American monsoon. *Journal of Climate*, *20*(9), 1792−1809.

Wang, J. R., & Schmugge, T. J. (1980). An empirical model for the complex dielectric permittivity of soils as a function of water content. *IEEE Transactions on Geoscience and Remote Sensing*, *18*, 288−295.

Yilmaz, M. T., Hunt, E. R. Jr, Goins, L. D., Ustin, S. L., Vanderbilt, V. C., & Jackson, T. J. (2006). Vegetation water content during SMEX04 from ground data and Landsat 5 Thematic Mapper imagery. *Remote Sensing of Environment* (in review).